

# CFD evaluation of drop retraction methods for the measurement of interfacial tension of surfactant-laden drops

Sachin Velankar,<sup>\*,1</sup> Hua Zhou, Hyun Kyoung Jeon, and Christopher W. Macosko

*Department of Chemical Engineering and Materials Science, University of Minnesota, Minneapolis, MN 55455, USA*

Received 27 May 2003; accepted 25 September 2003

## Abstract

Drop retraction methods are popular means of measuring the interfacial tension between immiscible polymers. Experiments show that two different drop retraction methods, imbedded fiber retraction (IFR) and deformed drop retraction (DDR), give inconsistent results when a surfactant is present on the surface of the drop. These inconsistencies are deemed to be due to dilution of the surfactant and due to gradients in interfacial concentration of surfactant along the drop surface. This physical picture is quantified for the simple case of a Newtonian drop in a Newtonian matrix, with an insoluble, nondiffusive surfactant at the interface. The drop is deformed in computational fluid dynamics simulations by shearing the matrix, and then allowed to retract. Dilution and interfacial tension gradients effects are found to be especially large at the early stages of retraction, making IFR unsuitable for measuring the interfacial tension of surfactant-laden interfaces. The effects of surfactant dilution and gradients are found to persist even at late stages of retraction, causing the DDR method to underestimate the equilibrium interfacial tension significantly. The largest underestimates occur when the drop viscosity is lower than the matrix viscosity. © 2003 Elsevier Inc. All rights reserved.

*Keywords:* Interfacial tension; Compatibilizer; Surfactant; Drop retraction; Fiber retraction; Marangoni stress; Adaptive remeshing

## 1. Introduction and motivation

Thermodynamically immiscible polymers are routinely blended together in order to improve their physical properties. When two immiscible polymer melts are blended, structural development is strongly affected by the interfacial tension between the polymers. The common methods of measuring the equilibrium interfacial tension between immiscible liquids, such as the pendant drop method or the spinning drop method, require that the drop shape achieve equilibrium before the measurement can be made. Due to the high viscosity of most polymers, the equilibration time can be very long, resulting in degradation of the polymer over the timescale of the measurement. Therefore, more rapid “dynamic” methods, which obtain the interfacial tension from the kinetics of interfacial evolution, have been developed for polymer melts. These methods are based on the principle that when a nonspherical inclusion of a liquid is suspended

in another immiscible liquid, it evolves into a spherical shape due to interfacial tension. This process is a balance between interfacial tension that drives interfacial evolution and the viscous resistance. Thus, the rate of interfacial evolution is proportional to the interfacial tension and offers a means of obtaining the interfacial tension. The interfacial evolution during the most common dynamic methods is shown in Fig. 1, and the relative merits of these methods have been reviewed recently [1].

Block copolymers are routinely employed to promote blending of immiscible polymers (e.g., by improving the dispersion of one polymer into another), and hence are commonly called “compatibilizers.” Compatibilizers are surface active, and lower the interfacial tension between the immiscible polymer melts. Due to this surfactant-like behavior of compatibilizers, the term “surfactant” will be used in this paper. The dependence of interfacial tension on block copolymer concentration has been the subject of numerous publications (see, for example, Retsos et al. [2] and references therein). In almost all such research, the interfacial tension was obtained by equilibrium methods. This cannot, however, be done for all polymers, especially not for high-molecular-weight polymers, due to the problem of degradation men-

\* Corresponding author.

*E-mail address:* [velankar@pitt.edu](mailto:velankar@pitt.edu) (S. Velankar).

<sup>1</sup> Present address: Department of Chemical and Petroleum Engineering, University of Pittsburgh, Pittsburgh, PA 15261, USA.

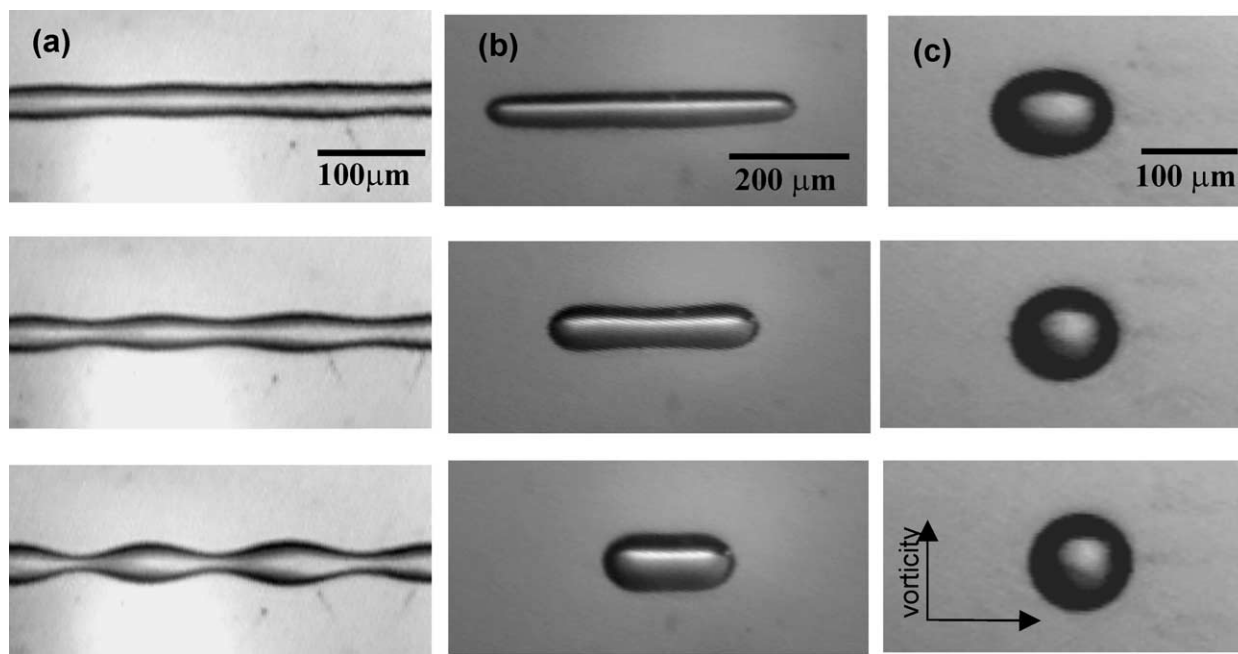


Fig. 1. Common dynamic methods of measuring interfacial tension between immiscible polymers illustrated for the uncompatibilized PE/PS system of Table 1 at 200 °C. Interfacial tension is obtained from the (a) rate of growth of a sinusoidal disturbance on a cylindrical fiber in the breaking thread method; (b) initial rate of retraction of a short fiber in the imbedded fiber retraction (IFR) method; (c) terminal rate of retraction of an ellipsoidal drop in the deformed drop retraction (DDR) method; (c) was obtained by applying a step strain (along the velocity direction shown) on a spherical drop, and then allowing it to retract.

tioned above. It is therefore tempting to employ dynamic methods to measure the interfacial tension of interfaces with block copolymers [3–5].

Accordingly, we attempted to measure the interfacial tension between polyethylene (PE) and polystyrene (PS), with added PS-*b*-PE diblock copolymer surfactant, using drop retraction methods. Since it was desirable to give the surfactant sufficient time to adsorb at the interface, the method suggested by Luciani et al. [6], which starts with an initially spherical drop, was chosen. The experimental procedure was to equilibrate an initially spherical drop for a certain amount of time, deform it by a step shear strain, and then allow it to retract back to its spherical shape. The main difference from Luciani's method is that we used a large step strain ( $\sim 5$ – $10$ ) to deform the drop, compared with the much smaller strains ( $<0.15$ ) used by Luciani [6]. One key advantage of the large step strain is that the viscoelastic relaxation of the polymer is mostly completed during the early retraction, allowing the assumption of Newtonian fluids to be made in the terminal stages of retraction. A second advantage of the large deforming strain is that the drop has sufficient time to become an *axisymmetric* ellipsoid before it retracts into a sphere, whereas this is generally not expected to be true in previous small shear strain experiments [6]. Axisymmetric ellipsoids are convenient when the retraction is observed along the velocity gradient direction, since the axes of the drop can be calculated from a conservation of volume equation without knowing the orientation angle of the major axis with respect to the flow direction. A final advantage is that early in the retraction process, the drop attains an approximately

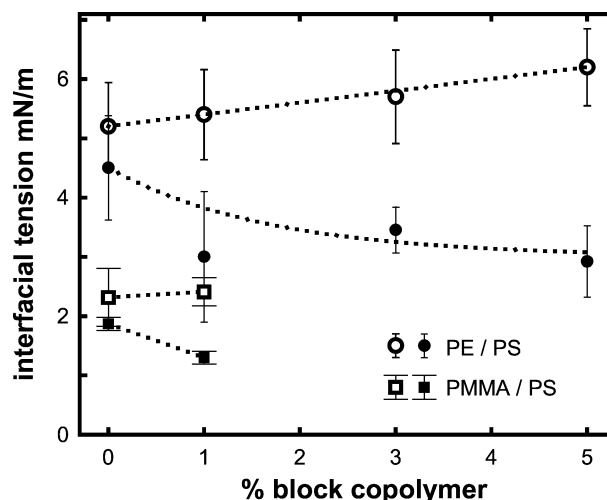


Fig. 2. Interfacial tension of compatibilized drops by DDR and IFR. Circles refer to the PE/PS system, whereas the squares refer to the PMMA/PS system. Open and filled symbols are interfacial tensions measured by IFR and DDR, respectively. Dotted lines are to guide the eye. Each point is the average of at least five experiments.

cylindrical shape [7–9] before becoming an axisymmetric ellipsoid. Therefore the initial cylindrical retraction can be analyzed using the imbedded fiber retraction (IFR) method and the terminal retraction of the ellipsoid by the deformed drop retraction method (DDR) method, thus allowing the interfacial tension to be obtained by both methods in the same experiment. Experimental details are given in Appendix A and the results of these experiments are shown in Fig. 2.

Table 1  
Properties of materials used

Drop/matrix	Polymers (supplier)	$M_n$ (kg/mol)	$M_w/M_n$	$\mu_0^*$ <sup>a</sup> (Pa s)	$\lambda^* = \mu_d/\mu_m$	$\sigma_0$ (mN/m)
PE/PS	PE (Dow HDPE 04452N)	18	4.8	1940	0.89	5.2 <sup>c</sup>
	PS (Dow, noncommercial)	65	2.2	2190		
	PS- <i>b</i> -PE	40; $f_{PS} = 0.5^b$	1.1	–		
PMMA/PS	PMMA (Scientific Polymer Products)	19	1.8	4470	0.56	1.2–1.9 <sup>d</sup>
	PS (Dow Styron 666D)	105	2.0	7990		
	PS- <i>b</i> -PMMA	34; $f_{PS} = 0.3$	1.4	–		

<sup>a</sup> Dynamic viscosity measured at 0.05 rad/s.

<sup>b</sup>  $f_{PS}$  = mole fraction of PS.

<sup>c</sup> Ref. [6].

<sup>d</sup> Refs. [25–27].

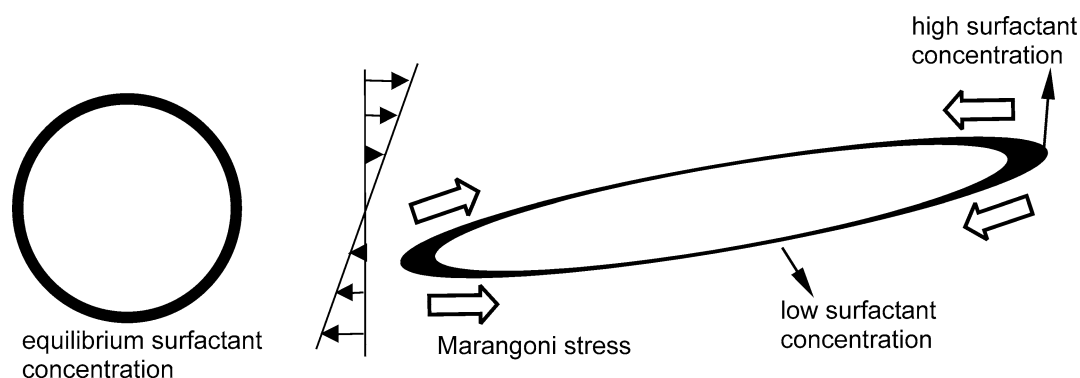


Fig. 3. Schematic of surfactant-laden drop after being deformed by a shear flow. Thickness of the black boundary of the drop represents the surfactant concentration. Initially, the spherical drop has a uniform, equilibrium concentration everywhere on its surface. Deformation causes low concentration at the waist of the drop and high concentration at the tips.

Without the diblock copolymer surfactant, the values of interfacial tension between PE and PS measured from IFR and DDR are comparable, and in reasonable agreement with the previously reported value in Table 1. However, for the system with surfactant, Fig. 2 shows that the interfacial tensions from IFR are far higher than those from DDR; indeed, IFR suggests that interfacial tension increases due to addition of surfactant, which is physically unrealistic. A similar result was observed for a polymethylmethacrylate (PMMA)/PS system with added PS-*b*-PMMA diblock copolymer surfactant; these data are shown in Fig. 2 as well.

In qualitative terms, the results of Fig. 2 may be explained by the physical picture in Fig. 3. When a surfactant-laden drop initially at equilibrium is subjected to a step deformation, the surfactant is convected by the applied flow field and is no longer uniformly distributed on the surface of the drop. In particular, if bulk diffusion is ignored (a good approximation considering the low diffusivity of most block copolymer surfactants), the concentration of the surfactant over most of the surface is lower than the equilibrium concentration, whereas the concentration at the tips is higher. Recent experiments have verified such concentration gradients directly using fluorescently labeled block copolymer [10], and indirectly by their effect on drop shapes [11]. Therefore, the waist of the drop tends to retract faster than expected from the equilibrium interfacial tension, whereas the tips tend to

retract more slowly. In addition, Marangoni stresses on the drop surface are expected to accelerate retraction. All of these effects are caused by deviations of the local concentration from the equilibrium value. Since these deviations are largest during the early stages of retraction, it is not surprising that IFR and DDR give different values for the interfacial tension.

These experiments motivated the present work, in which we attempt to make the above physical picture more quantitative. In particular, the question addressed here is: Are dynamic methods of measuring interfacial tension still applicable when a surfactant is present at the interface between the immiscible fluids?

For the breaking thread method, the linear stability analysis of Hansen et al. [12] has already demonstrated that the surfactant affects the kinetics of interfacial evolution significantly. In particular, they have shown that if the thread viscosity is significantly different from the matrix viscosity, the wavelength of the disturbance is significantly smaller than expected, and its initial growth rate is significantly smaller than expected from the equilibrium value of the interfacial tension. Thus, although the authors did not mention the relevance of their results to the breaking thread method explicitly, their analysis indicates that this method can greatly underestimate the interfacial tension of surfactant-laden threads.

In this paper, the effect of surfactant on the kinetics of IFR and DDR is studied by numerical simulation and the validity of these methods for measuring the interfacial tension of surfactant-laden drops is assessed. The deformation history in the simulations is the same as in the experiments of Fig. 2: a shear strain is applied to an initially spherical drop, followed by retraction under quiescent conditions. As mentioned above, this offers a means of obtaining the interfacial tension by both methods, IFR and DDR, in a single experiment.

## 2. Problem statement

### 2.1. Governing equations

An initially spherical drop of radius  $R_0$  and viscosity  $\mu_d$  is suspended in an immiscible liquid matrix of viscosity  $\mu_m$ . Both fluids are assumed incompressible, and inertial and buoyancy effects are assumed to be small in both phases, which are excellent assumptions for high-viscosity polymer melts. In addition, both fluids are assumed Newtonian. Although polymer melts are often strongly viscoelastic, interfacial-tension-driven retraction is generally sufficiently slow to permit the assumption of Newtonian behavior. Thus, bulk flow in each phase is described by the Stokes flow equations,

$$\nabla \cdot \mathbf{u}_i = 0, \quad \nabla \cdot \mathbf{T}_i = 0, \quad i = d \text{ (drop) or } m \text{ (matrix)}, \quad (1)$$

$$\mathbf{T}_i = -p_i \mathbf{I} + \mu_i (\nabla \mathbf{u}_i + \nabla \mathbf{u}_i^T), \quad i = d \text{ or } m, \quad (2)$$

where  $\mathbf{u}_i$  and  $p_i$  are the velocity and pressure fields respectively,  $\mathbf{T}_i$  is the stress tensor, and  $\mathbf{I}$  is the identity tensor.

The simulation consists of subjecting the drop to shear flow at a rate of  $\dot{\gamma}$  for a certain time  $t_F$ , and then stopping the shear flow and allowing the drop to retract. Thus, far away from the drop, the velocity field is

$$\mathbf{u}_m(\mathbf{x}, t) = \begin{cases} \begin{pmatrix} 0 & \dot{\gamma} & 0 \\ 0 & 0 & 0 \\ 0 & 0 & 0 \end{pmatrix} \cdot \mathbf{x} & \text{for } 0 \leq t < t_F, \\ 0 & \text{for } t_F < t. \end{cases} \quad (3)$$

The problem statement is completed by specifying the boundary conditions of no slip, and of discontinuity of stress at the drop surface,

$$\mathbf{u}_d = \mathbf{u}_m, \quad (4)$$

$$(\mathbf{T} \cdot \mathbf{n})_m - (\mathbf{T} \cdot \mathbf{n})_d = \sigma \kappa \mathbf{n} - \nabla_S \sigma, \quad (5)$$

where  $\kappa$  is the local mean curvature,  $\mathbf{n}$  is the local outward normal, and  $\nabla_S = (\mathbf{I} - \mathbf{nn}) \cdot \nabla$  is the gradient operator on the surface.

The dependence of the local interfacial tension,  $\sigma$ , on the local surfactant concentration,  $\Gamma$ , is defined by the Langmuir equation of state,

$$\sigma = \sigma_0 + RT\Gamma_\infty \ln\left(1 - \frac{\Gamma}{\Gamma_\infty}\right), \quad (6)$$

where  $\sigma_0$  is the interfacial tension of the bare interface without surfactant, and  $\Gamma_\infty$  is the maximum possible interfacial concentration of surfactant. A key feature of the Langmuir equation shown in Fig. 4 is that with increasing surfactant concentration  $\Gamma$ , the interfacial tension decreases increasingly rapidly as  $\Gamma_\infty$  is approached. This feature captures the behavior of many low-molecular-weight surfactants qualitatively. This constitutive equation has not been evaluated for polymeric surfactants such as block copolymers; however, Appendix B demonstrates that the results of this paper are not conditional on the Langmuir equation being valid; the results appear to be valid quantitatively regardless of constitutive equation.

The surfactant is assumed to be insoluble (i.e., total amount of surfactant on the drop is fixed), and diffusion of surfactant along the interface is neglected. The above equation of state and the conditions under which bulk solubility and surface diffusion can be neglected have been discussed in detail previously [10–14].

### 2.2. Dimensionless quantities

All dimensionless quantities are superscripted by an asterisk. The viscosity ratio  $\lambda^*$  is defined as

$$\lambda^* = \frac{\mu_d}{\mu_m}. \quad (7)$$

The equilibrium concentration  $\Gamma_e$  everywhere on the spherical drop under quiescent conditions, and the corresponding equilibrium interfacial tension  $\sigma_e$  are related by Eq. (6),

$$\frac{\sigma_e}{\sigma_0} = 1 + \frac{RT\Gamma_\infty}{\sigma_0} \ln\left(1 - \frac{\Gamma_e}{\Gamma_\infty}\right) = (1 + E_0^* \ln(1 - c^*)), \quad (8)$$

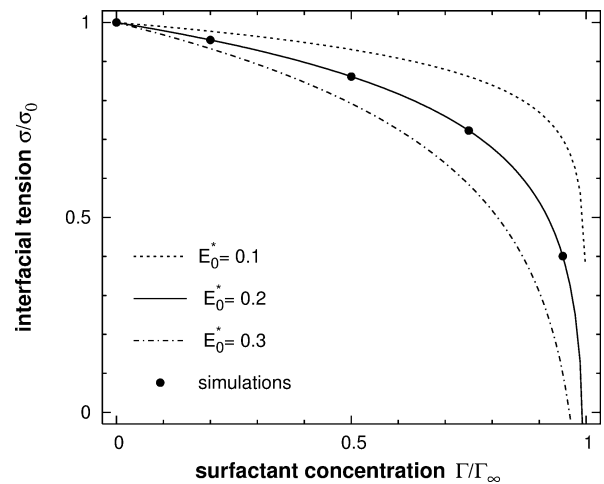


Fig. 4. Interfacial tension vs concentration of surfactant  $\Gamma/\Gamma_\infty$  per Langmuir equation, Eq. (6). Increasing  $E_0^* = RT\Gamma_\infty/\sigma_0$  makes the interfacial tension increasingly sensitive to surfactant concentration. Simulations were performed for the filled circles with  $E_0^* = 0.2$  and  $c^* = \Gamma_e/\Gamma_\infty = 0, 0.2, 0.5, 0.75, \text{ and } 0.95$ .

where

$$E_0^* = \frac{RT\Gamma_\infty}{\sigma_0} \quad \text{and} \quad c^* = \frac{\Gamma_e}{\Gamma_\infty}. \quad (9)$$

$c^*$  is the dimensionless equilibrium surface concentration, or surface coverage.  $E_0^*$ , along with  $\Gamma_\infty$ , is a characteristic property of a particular surfactant and the bulk fluids. Note that the present definition of  $E_0^*$  was preferred over that of Eggleton et al. [15] because  $E_0^*$  and  $\Gamma_e$  (or equivalently  $E_0^*$  and  $c^*$ ) can be varied independently. In the present simulations,  $E_0^*$  was fixed and  $c^*$  was varied. This is analogous to the experiments of Fig. 2 in which the polymers and the surfactant were fixed and the concentration of the surfactant was increased.

The equilibrium interfacial tension and concentration,  $\sigma_e$  and  $\Gamma_e$ , respectively, are used to define the dimensionless local concentration,  $\Gamma^*$ , and the dimensionless local interfacial tension,  $\sigma^*$ :

$$\Gamma^* = \frac{\Gamma}{\Gamma_e}, \quad \sigma^* = \frac{\sigma}{\sigma_e}. \quad (10)$$

Equation (6) can therefore be written in dimensionless form as

$$\sigma^* = \frac{1 + E_0^* \ln(1 - c^* \Gamma^*)}{1 + E_0^* \ln(1 - c^*)}. \quad (11)$$

During the deformation phase, the appropriate dimensionless variables are

$$Ca^* = \frac{R_0 \mu_m \dot{\gamma}}{\sigma_e}, \quad t^* = \dot{\gamma} t, \quad (12)$$

where  $Ca^*$  is the capillary number, and  $t^*$  is the dimensionless time during shear flow, or equivalently, the shear strain.

During the retraction phase, dimensionless time is defined as

$$t^* = \frac{t \sigma_e}{R_0 \mu_m}. \quad (13)$$

### 2.3. Parameter values

The range of viscosity ratios studied is from  $\lambda^* = 0.01$  to  $\lambda^* = 3$ . Significantly larger values of  $\lambda^*$  are not interesting experimentally because of the increasing difficulty of deforming drops in shear flow as  $\lambda^*$  exceeds 3. Values of  $\lambda^*$  lower than 0.01 show asymptotic behavior, with the deformation and retraction behavior being dictated by the matrix viscosity, and the drops behaving as though they were inviscid.

In all simulations,  $Ca^* = 1$  and the drops were deformed to a strain of  $\dot{\gamma} t_F = 1$  or 5. Note that in our experiments,  $Ca^* \gg 1$  and  $\dot{\gamma} t_F \sim 5$ –10; however, the high curvature resulting from  $Ca^* \gg 1$  is computationally expensive, and hence  $Ca^* = 1$  was chosen for simulations. However, limited simulations at  $\lambda^* = 1$  using  $Ca = 10$  and 100 showed no qualitative changes in the results.

The calculations of Eggleton et al. [16] suggest that  $E_0^* = 0.2$  is reasonable for low-molecular-weight surfactants. There are only limited results suggesting that Eq. (6) is valid for polymeric surfactants [28]. Nevertheless, a value of 0.2 is not unreasonable for polymeric surfactants as shown by a simple calculation: The maximum concentration of block copolymer at an interface is of the order of 0.1 molecule/nm<sup>2</sup> [17]. With a bare interfacial tension of about 5 mN/m and a temperature of 200 °C this corresponds to  $E_0^* \sim 0.15$ . Therefore  $E_0^* = 0.2$  was used in all the simulations. This value is somewhat lower than the value of 0.38 obtained by Hu and Lips [28].

Simulations were performed for surface coverages of  $c^* = 0, 0.2, 0.5, 0.75$ , and 0.95; the  $c^* = 0$  case (no surfactant) was used as a reference.

### 2.4. Numerical techniques

Drop shapes were obtained using a 3-D adaptive meshing FEM algorithm under development. Pressure stabilized Petrov–Galerkin (PSPG) formulation was used to allow equal order interpolation of velocity and pressure with linear tetrahedral elements [18,19,29,30]. Message Passing Interface (MPI) was used for efficient parallelization. The initial mesh was generated using HyperMesh, a commercial program from Altair Engineering. After the deformation at each time step, both the surface and volume meshes are remeshed to ensure accurate resolution of surface curvature and other variables. Details of the numerical method can be found elsewhere [18,19]. Here surfactants are assumed to be insoluble, whereas Zhou et al. [18] have considered the more general case of surfactants that are soluble in the bulk phases.

## 3. Results

The results for  $\lambda^* = 1$  and  $c^* = 0, 0.2$ , and 0.95 will first be presented in detail. The results for the other values of  $c^*$  and for  $\lambda^* \neq 1$  will be summarized later in the paper.

### 3.1. Fiber retraction for $\lambda^* = 1$

Fig. 5 shows the shapes of drops with  $c^* = 0, 0.2$ , and 0.95 during retraction. Fig. 6 shows the evolution of the three axes for the corresponding drops. Here  $R_1$  and  $R_2$  are the major and minor axes, respectively, and  $R_3$  is the axis along the vorticity direction. The general features of the deformation and retraction process, consistent with previous observations [9], are as follows. The shear strain applied from  $t^* = 0$  to  $t^* = 5$  is seen to increase  $R_1$  somewhat less than expected if deformation were affine. This is attributable to the fact that affine deformation is expected as  $Ca^* \rightarrow \infty$ , whereas  $Ca^* = 1$  during deformation, and hence the drop has time to retract during deformation itself. The  $R_2$  axis decreases sharply after deformation begins, whereas the  $R_3$  axis decreases more slowly because this decrease is entirely

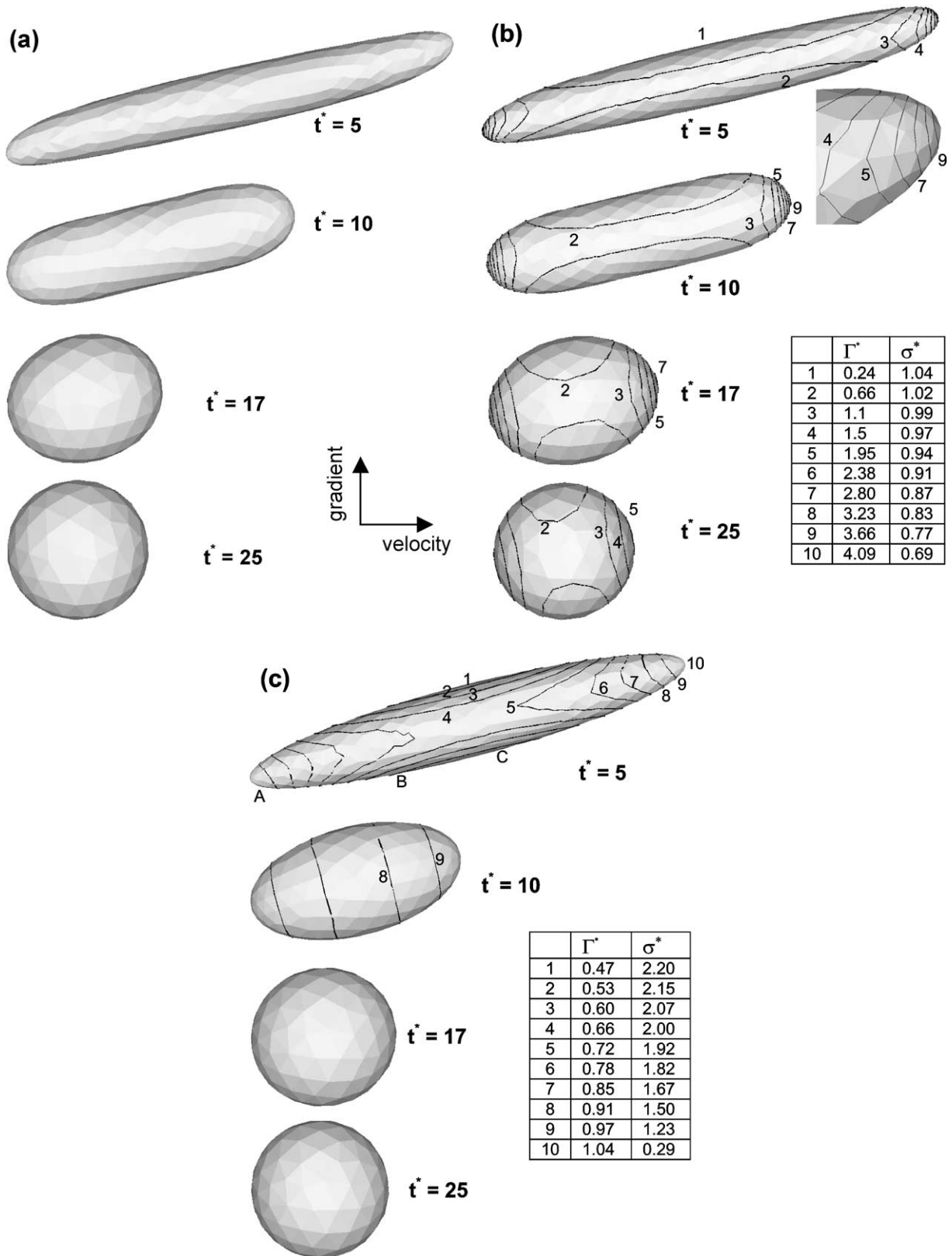


Fig. 5. Shapes of drops with (a)  $c^* = 0$ , (b)  $c^* = 0.2$ , and (c)  $c^* = 0.95$  at various times during retraction after shearing at  $Ca^* = 1$  to a strain of 5. The velocity and gradient directions in (a) apply to (b) and (c) as well. The contour lines on the surface in (b) and (c) mark the local concentration as tabulated. The magnified image in (b) shows a detailed view of the tip of the drops at  $t^* = 5$ . The drops at  $t^* = 17$  and 25 in (c) have no contour lines, since concentration everywhere on the drop is very close to 1.

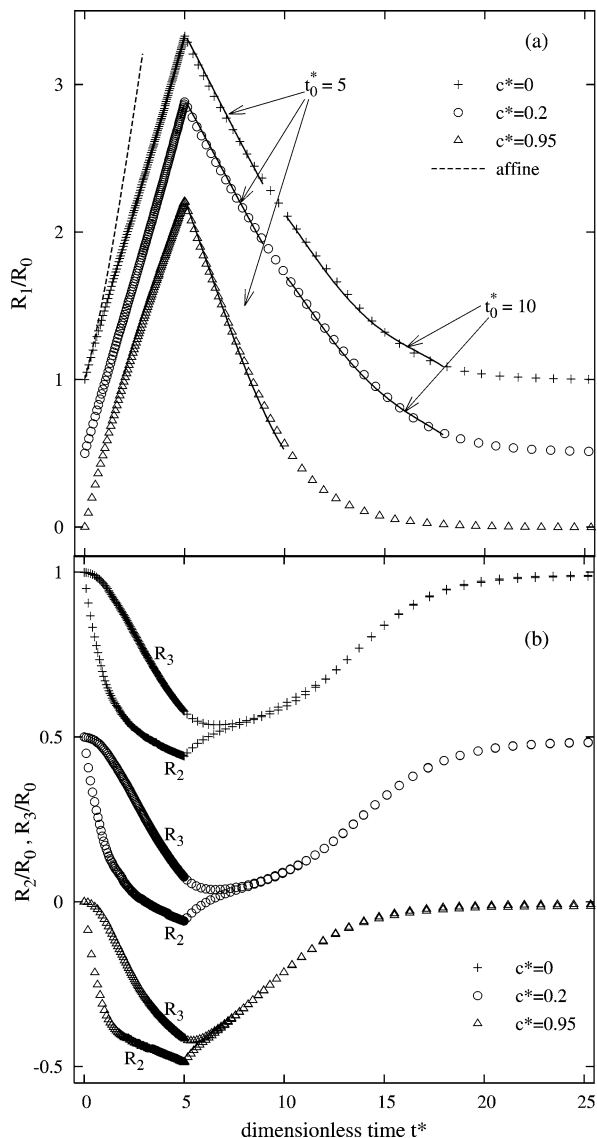


Fig. 6. Axes of drops during deformation and retraction. The y-axes refers to the  $c^* = 0$  curve only; the  $c^* = 0.2$  and  $c^* = 0.95$  curves have been shifted downward by 0.5 and 1 units, respectively, for clarity. Dashed line in (a) is the  $R_1/R_0$  for affine deformation of the  $c^* = 0$  drop. Solid lines in (a) are the calculations of Tjahjadi et al. Eq. (16) starting with the drop shapes at  $t^* = 5$  and  $t^* = 10$  for  $c^* = 0$  and  $c^* = 0.2$ , and at  $t^* = 5$  for  $c^* = 0.95$ .

due to interfacial tension, and not due to the applied flow field. Upon cessation of shear,  $R_1$  decreases rapidly, whereas  $R_2$  increases as the drop retracts into a sphere. The behavior of  $R_3$  is somewhat more complex, yet after a certain time following cessation of shear,  $R_3$  also increases monotonically. For  $t^* > 8$ ,  $R_2 \approx R_3$  for all drops in Fig. 6, i.e., the drops become axisymmetric. Moreover, Fig. 5 shows that for  $c^* = 0$  and 0.2, at  $t^* = 10$ , the drop shapes can be well-represented by a cylinder with hemispherical endcaps at short times. Therefore the applicability of the IFR method can be evaluated for these drops starting at  $t^* \approx 10$ .

Tjahjadi et al. [20] have solved the retraction of cylindrical drops with hemispherical endcaps by boundary integral

methods and presented the time-evolution of the dimensionless drop half-length  $R_1/R_0$  as a power series in time,

$$\frac{R_1}{R_0} = \sum_{n=0}^4 k_n \left( \frac{\sigma(t-t_0)}{\mu_m a(t_0)} \right)^n \quad \text{for } t \geq t_0, \quad (14)$$

where  $t_0$  is the “starting time of the fiber retraction,” i.e., some convenient time at which the fiber may be approximated as a cylinder with hemispherical endcaps.  $a(t_0)$  is the initial radius of the corresponding cylinder defined by volume conservation,

$$\frac{4}{3}\pi R_0^3 = 2\pi a(t_0)^2 R_1 - \frac{2}{3}\pi a(t_0)^3. \quad (15)$$

The coefficients  $k_n$  have been tabulated as a function of the viscosity ratio  $\lambda^*$  and the initial aspect ratio,  $R_1(t_0)/a(t_0)$ , of the cylinder [20]. Experimentally, some time when the shape of the fiber is approximately cylindrical with hemispherical endcaps is taken as  $t_0$ , and  $a(t_0)$  is calculated from Eq. (15) to obtain the initial aspect ratio, and hence  $k_n$ . Varying  $\sigma$  to fit the experimental  $R_1/R_0$  vs time data allows determination of the interfacial tension using the fiber retraction method. In the present situation, we seek to treat the simulations like experimental data, i.e., fit the equation

$$\frac{R_1}{R_0} = \sum_{n=0}^4 k_n \left( \frac{\sigma_{\text{app}}(t-t_0)}{\mu_m a(t_0)} \right)^n \quad \text{for } t \geq t_0 \quad (16)$$

to the simulated data and compare the apparent interfacial tension,  $\sigma_{\text{app}}$ , with the equilibrium value,  $\sigma_e$ . Since simulations are in terms of dimensionless quantities, the above equation can be rewritten as

$$\begin{aligned} \frac{R_1}{R_0} &= \sum_{n=0}^4 k_n \left( \frac{\sigma_{\text{app}}}{\sigma_e} \frac{\sigma_e(t-t_0)}{\mu_m R_0} \frac{R_0}{a(t_0)} \right)^n \\ &= \sum_{n=0}^4 k_n \left( \frac{\sigma_{\text{app}}}{\sigma_e} (t^* - t_0^*) \frac{R_0}{a(t_0^*)} \right)^n \quad \text{for } t^* \geq t_0^*, \end{aligned} \quad (17)$$

where  $t_0^*$  is the dimensionless starting time of fiber retraction. Equation (17), with  $\sigma_{\text{app}}/\sigma_e$  as a fitting parameter, can be used to fit the simulated  $R_1/R_0$  vs  $t^*$  results. The best fit value of  $\sigma_{\text{app}}/\sigma_e$  is then an indication of how accurately IFR measures the equilibrium interfacial tension. Taking  $t_0^* = 10$ , the initial aspect ratio is found from the drop shape at this time, and the corresponding  $k_n$ 's found from Tjahjadi et al. [20]. Fig. 5 shows that the best fit of Eq. (17) is obtained with  $\sigma_{\text{app}}/\sigma_0$  of 0.98. Thus, IFR is able to measure the interfacial tension of surfactant-free drops within 2% error. Remarkably, using  $t_0^* = 5$  (cessation of shear) as the start of “fiber” retraction also yields a best fit of Eq. (17) with  $\sigma_{\text{app}}/\sigma_0$  of 0.98 although the drop is not an axisymmetric cylinder ( $R_2 \approx R_3$  is not true) at this time. This suggests that the retraction of  $R_1$  is not very sensitive to the details of the initial drop shape as long as the aspect ratio is large. In any case, the main conclusion is that the interfacial tension of surfactant-free drops can be measured accurately by IFR.

The initial retraction of the  $c^* = 0.2$  drop is almost identical to that of the  $c^* = 0$  drop. Fitting Eq. (17) (with either  $t_0^* = 5$  or with  $t_0^* = 10$ ) yields  $\sigma_{\text{app}}/\sigma_e(c^* = 0.2) = 0.95$ . Thus,  $\sigma_e$  of the  $c^* = 0.2$  drop is estimated within 5% error by the IFR method. At first glance this appears to be a tolerable error. However the equilibrium interfacial tension of this drop is only 4% lower than of the bare interface, i.e.,  $\sigma_e(c^* = 0.2) = 0.96\sigma_0$ . Thus, the error in measuring the equilibrium interfacial tension by IFR (5%) is comparable to the decrease in interfacial tension from that of the bare interface (4%). Clearly, the IFR is not a suitable method to measure the small decreases in equilibrium interfacial tension when the surfactant is present in dilute quantities.

The initial retraction of the drop with  $c^* = 0.95$  is significantly faster than that of the other two drops shown in Fig. 6; indeed this is evident even from the drop shapes in Fig. 5. Fitting Eq. (17) with  $t_0^* = 5^2$  yields  $\sigma_{\text{app}}/\sigma_e(c^* = 0.95) = 1.5$ , i.e., the IFR method overestimates the equilibrium interfacial tension by 50% for the  $c^* = 0.95$  drop. What is the reason for this unexpectedly fast retraction of the  $c^* = 0.95$  drop and the resulting error in estimated interfacial tension?

One possibility is the qualitative change in the drop shape: the drop shape is ellipsoidal rather than cylindrical at early times. The noncylindrical shape of the drop is not likely to be the cause for the faster retraction; indeed earlier in this section, it was noted that the retraction of  $R_1$  is rather insensitive to the initial shape. The most probable reason for the fast initial retraction is evident from Fig. 5c which shows the interfacial concentration on the drop. It is clear that at  $t^* = 5$ ,  $\Gamma^*$  ranges from 0.5 to 0.9, i.e., the interfacial concentration  $\Gamma$  over most of the drop surface is from about 0.5 to 0.9 times  $\Gamma_e$ . The corresponding values of  $\sigma^*$  from Eq. (11) range from 1.5 to 2.1, i.e., most of the drop surface has an interfacial tension that is from 1.5 to 2.1 times the equilibrium value. Moreover, the  $c^* = 0.95$  drop also has a sharp gradient in interfacial tension, i.e., a Marangoni stress, close to its tips. An approximate comparison of the magnitude of the Marangoni stresses and of the capillary pressure may be made by comparing  $\nabla_s \sigma$  and  $\kappa \sigma$  along the ABC contour in the top figure in Fig. 5c. These two quantities are found to be nearly equal at the tips of the drop, i.e., the magnitude of the Marangoni stress is nearly equal to the magnitude of the capillary pressure. Thus, the Marangoni stress is sufficiently large to accelerate the retraction of the tips significantly. To summarize, the initial retraction over most of the drop surface is driven by an interfacial tension that is considerably higher than  $\sigma_e$ ; in addition, it is enhanced by Marangoni stresses at the tips. Therefore the Tjahjadi et al. prediction significantly overestimates the interfacial tension.

The results of Fig. 6 highlight the pitfalls of using dynamic methods to measure the interfacial tension of surfactant-laden interfaces. A dynamic method is one that

uses the kinetics of interfacial evolution to measure the interfacial tension. For a surfactant-laden interface, interfacial evolution is generally accompanied by a change in the interfacial tension, as well as by gradients in surfactant concentration. Thus, the local interfacial tension at any point on the interface is generally different from the equilibrium interfacial tension. Therefore, a dynamic method will, in general, yield an interfacial tension that is different from the equilibrium interfacial tension. For the shear history followed here, deviations of interfacial tension from the equilibrium value, are largest at early times, making the initial retraction most susceptible to these effects. Clearly, using the initial retraction of the drop to obtain the interfacial tension of surfactant-laden drops is not advisable.

### 3.2. DDR for $\lambda^* = 1$

Figs. 5 and 6b show that at long times, all drops are slightly deformed ellipsoids. Therefore the applicability of the DDR method can be evaluated using the last stages of retraction. The DDR method obtains the interfacial tension from the relaxation time,  $t_d$ , of a slightly deformed drop. Experimentally, the relaxation time is obtained by plotting the deformation parameter as a function of time. In the terminal stages of retraction, the drop is ellipsoidal and the deformation parameter  $D$  decreases exponentially with time [6]:

$$D = \frac{R_1 - R_2}{R_1 + R_2} = D_0 \exp\left(-\frac{t}{t_d}\right). \quad (18)$$

In dimensionless terms, this may be rewritten as

$$D = D_0 \exp\left(-\frac{t\sigma_e}{\mu_m R_0} / \frac{t_d\sigma_e}{\mu_m R_0}\right) = D_0 \exp\left(-\frac{t^*}{t_d^*}\right), \quad (19)$$

where  $t_d^*$  is the dimensionless relaxation time of a slightly deformed drop. For a surfactant-free drop, Taylor's theory predicts [6]

$$t_d^* = \frac{t_d\sigma_e}{R_0\mu_m} = \frac{(19\lambda^* + 16)(2\lambda^* + 3)}{40(\lambda^* + 1)}. \quad (20)$$

Thus, once  $t_d$  is determined from experimental data using Eq. (18), Eq. (20), along with independent measurements of  $R_0$ ,  $\mu_m$ , and  $\lambda^*$ , yields the interfacial tension. This procedure constitutes the DDR method. The questions addressed in this section are: do the gradients in surfactant concentration caused by the initial shearing have an effect during late stages of retraction? In particular, is terminal retraction still exponential as per Eq. (19)? If so, is  $t_d^*$  still given by Eq. (20), with  $\sigma$  being replaced simply by the equilibrium interfacial tension  $\sigma_e$ ? Note that if terminal retraction is still exponential and Eq. (20) is still valid for a surfactant-laden interface, DDR can be used to measure  $\sigma_e$  from  $\tau_d$ ; i.e., the use of the DDR method to measure the equilibrium interfacial tension of surfactant-laden drops is justified.

Fig. 7 replots the results of the deformation and retraction in the form required for the DDR method. The general features of this plot are as follows: for the surfactant-free drop,

<sup>2</sup> A fit starting with the shape at  $t_0^* = 10$  was not done since at  $t_0^* = 10$ , the drop is not sufficiently elongated to be approximated as a cylinder.

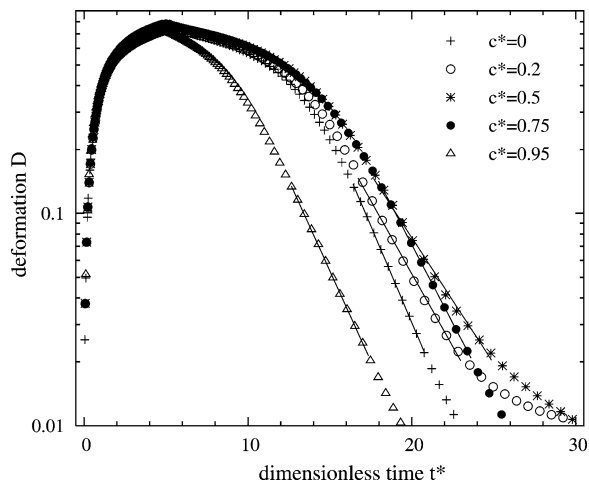


Fig. 7. Deformation parameter of drops with  $\lambda^* = 1$  during deformation and retraction. Deformation occurs at  $Ca^* = 1$  to a shear strain of 5. Solid lines are exponential fits to points with  $0.02 < D < 0.15$  and are used to obtain the dimensionless drop relaxation times. The points at  $c^* = 0$ ,  $c^* = 0.2$ , and  $c^* = 0.95$  are the same as in Fig. 6, plotted differently.

the deformation parameter increases during shearing, and then decreases during retraction. During the initial stages of retraction the deformation parameter decreases slowly. Once the drop shape can be well represented by a slightly deformed ellipsoid, the deformation parameter decreases exponentially with time. Addition of surfactant causes three qualitative changes. For  $c^* = 0.2$ , a new relaxation process is evident at very long times when the deformation parameter decays more slowly than the exponential relaxation. This slow relaxation becomes faster as  $c^*$  is increased to 0.5, and is no longer visible when  $c^*$  is further increased to 0.75. Finally, for  $c^* = 0.95$ , the initial retraction is greatly accelerated; this has already been discussed in the previous section.

The slow relaxation process at long times, and its behavior with increasing  $c^*$ , can be explained as follows. The surfactant-laden drop retracts under the influence of two driving forces: differences in capillary pressure between the tips and the waist, and Marangoni stresses. The capillary pressure is the product of the local curvature,  $\kappa$ , and the local interfacial tension,  $\sigma$ . The curvature is higher at the tips than at the waist, however, the interfacial tension is lower at tips than the waist. Therefore, at some time during the retraction process, the product  $\kappa\sigma$ , which is capillary pressure, is equal at the tips and at the waist. Beyond this time, further retraction is driven by Marangoni stresses alone. At  $c^* = 0.2$ , Fig. 4 shows that the interfacial tension is depends only weakly on concentration, thus Marangoni stresses are weak. Thus, retraction is driven by Marangoni stress alone, and the corresponding relaxation of concentration gradients, occurs very slowly. Indeed, at  $t^* = 25$ , Fig. 5b shows that although the drop is almost completely spherical, a significant concentration gradient, corresponding to a small interfacial tension gradient, still exists along the surface. With increasing  $c^*$ , the interfacial tension becomes increasingly sensitive to concentration, leading to stronger Marangoni stresses, thereby

accelerating the slow process. Thus, to summarize, the origin of the second relaxation process is the fact that for a surfactant-laden drop, capillary pressure cannot drive retraction beyond a certain time; the slow process accelerates with increasing  $c^*$  due to the increasing strength of Marangoni stresses.

The DDR method is based on obtaining the time constant of the exponential decrease of the deformation parameter, and using Taylor's Eq. (20) for this time constant to obtain the interfacial tension. At low surfactant concentrations, the exponential relaxation gives way to a slower relaxation at long times; thus there is some arbitrariness in choosing an "exponentially decreasing" portion of the deformation vs time data. We choose the range  $0.02 < D < 0.15$ ; this range is typical of experiments since deformations less than 0.02 are difficult to measure reliably, whereas exponential decay generally does not begin before  $D < 0.15$ . The exponential fits are shown in Fig. 7 and the corresponding dimensionless relaxation times are plotted in Fig. 8.

Fig. 8a shows that the dimensionless terminal relaxation times of the surfactant-laden drops are larger than the Taylor value predicted by Eq. (20). The largest dimensionless relaxation time occurring at  $c^* = 0.5$  is about 70% larger than the Taylor theory; thus using DDR would underestimate the equilibrium interfacial tension of the  $c^* = 0.5$  drop by 70%. The data of Fig. 8a have been replotted in Fig. 8b in terms of an apparent interfacial tension vs surfactant concentration, i.e., in a form similar to that of Fig. 2 (except that Fig. 2 has bulk concentration on the  $x$ -axis). This may be done by using Eq. (20) to obtain apparent values of interfacial tension from the  $t_d^*$  values obtained from the simulations, i.e., by rewriting Eq. (20) as

$$\begin{aligned} \sigma_{\text{app}} &= \frac{R_0 \mu (19\lambda^* + 16)(2\lambda^* + 3)}{t_d 40(\lambda^* + 1)} \\ &= \frac{\sigma_e (19\lambda^* + 16)(2\lambda^* + 3)}{t_d^* 40(\lambda^* + 1)}, \end{aligned} \quad (21)$$

where  $\sigma_e$  is obtained from Eq. (8). It is seen that for  $c^* = 0.5$ , the apparent interfacial tension measured by DDR is considerably lower than the equilibrium interfacial tension as mentioned above. Fig. 8b also plots the apparent interfacial tension obtained for the  $c^* = 0.95$  drop from IFR (see Fig. 6a), which is about 50% larger than the equilibrium value, as mentioned in the previous section. Thus, the simulations are able to reproduce the experimental observation of Fig. 2 that the interfacial tension obtained from IFR is considerably larger than that obtained from DDR.

However, Fig. 2 also shows that the apparent interfacial tension from IFR with large amounts of surfactant is larger than the bare interfacial tension. In other words, the surfactant-laden drop retracts, not only faster than expected from its equilibrium interfacial tension, but even faster than expected from the bare interfacial tension. Such fast retraction was not observed in any of the simulations, even at the highest value of  $c^* = 0.98$  studied (not shown).

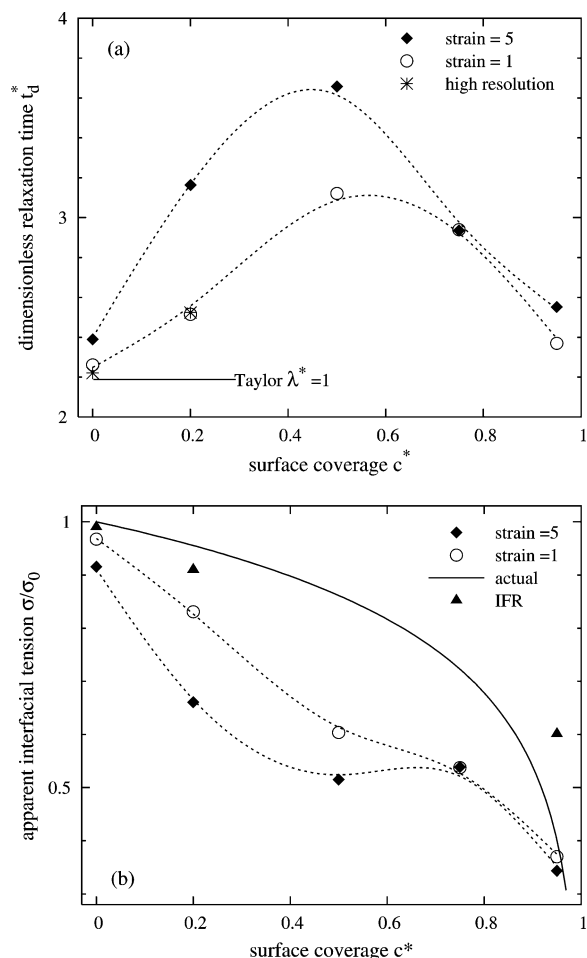


Fig. 8. (a) Dimensionless drop relaxation times  $t_d^*$  for  $\lambda^* = 1$ . Points obtained from fitting  $\log(D)$  vs  $t_r$  data with  $0.02 < D < 0.15$  to exponential fits (shown in Fig. 7 for strain = 5; not shown for strain = 1). Broken lines are guides to the eye. Solid line is Eq. (20) for  $\lambda^* = 1$ . Points at  $c^* = 0$  and 0.2 marked "high resolution" correspond to a larger mesh size of 200 points on the initially spherical drop (vs 115 points for all the other simulations). These demonstrate that the simulations have adequate resolution. (b) Apparent interfacial tension measured by DDR. Open circles and solid diamonds are results of (a) recast in the form of apparent interfacial tension per Eq. (21). Broken lines are guides to the eye. Solid triangles are the apparent interfacial tension from IFR per Fig. 6a. The solid line is the equilibrium interfacial tension, Eq. (8); deviation of the points from this line represents error in measuring the equilibrium interfacial tension.

### 3.3. DDR at $\lambda^* \neq 1$

The retraction behavior of droplets with viscosity ratio other than 1 is now presented. For these simulations, a shear strain of 1 was used to deform the droplets, rather than the value of 5 used in the previous section. The reasons for this are as follows. First, it has already been shown that the IFR method is not suitable to measure the equilibrium interfacial tension of surfactant-laden drops because the large interfacial deformation and retraction involved in the procedure causes large deviations in interfacial tension from the equilibrium value. Thus, one motivation for using a deforming strain of 5, viz., the ability to use IFR and DDR in a single

experiment, is no longer valid. Second, the large interfacial curvature caused by a strain of 5 makes these simulations computationally intensive; this problem is expected to be exacerbated for  $\lambda^* \ll 1$ . In contrast, simulations with a strain of 1 take considerably less computational effort. Finally, limited experiments for  $\lambda^* < 1$  show that surfactant-laden drops deformed by large strains can have strongly nonellipsoidal (or noncylindrical) shapes. In particular, stretched-out tips were observed during retraction at  $\lambda^* = 0.25$  in our research, and have been noted previously at  $\lambda^* = 1$  [11]. Such drop shapes are unsuitable for interfacial tension measurements. For all these reasons, it is desirable to keep the deforming strain low for  $\lambda^* < 1$  in the simulations; accordingly this section presents deformation–retraction simulations with a strain of 1.

The deformation vs  $t^*$  results for a strain of 1 and for various values of  $\lambda^*$  show all the qualitative features of Fig. 7: for  $c^* = 0$ , the terminal relaxation is exponential, whereas for nonzero values of  $c^*$ , two relaxations processes are seen: a faster one corresponding to shape retraction of ellipsoidal drops, and a slower one corresponding to relaxation of concentration gradients on the drop surfaces. Due to their similarity to Fig. 7, these results are not shown here. These  $D$  vs  $t^*$  results are treated similarly to those in Fig. 7: the points with  $0.02 < D < 0.15$  are fitted to exponential decays to obtain the relaxation times.

The case of  $\lambda^* = 1$  is considered first to demonstrate that the retraction behavior is similar qualitatively, regardless of whether the shear strain is 5 or 1. For  $\lambda^* = 1$ , these relaxation times for a shear strain of 1 are compared with the relaxation times for a shear strain of 5 in Fig. 8. It is seen that the dependence of the dimensionless relaxation time on the equilibrium surfactant concentration is similar for deforming strains of 1 and 5; however, the deviations from Taylor's theory are smaller for a shear strain of 1. This suggests that if DDR is to be used to measure the interfacial tension of compatibilized drops, the deforming strain should be kept as small as possible. The main disadvantage of decreasing the deforming strain are that in polymeric systems, there is not sufficient time for viscoelastic relaxation of the bulk before exponential retraction begins.

Only the  $c^* = 0$  and  $c^* = 0.5$  cases have been simulated for  $\lambda^* \neq 1$ . The dimensionless relaxation times (once again obtained by fitting the points with  $0.02 < D < 0.15$  to exponential relaxations) are plotted as a function of  $\lambda^*$  in Fig. 9. The relaxation times for the  $c^* = 0$  drops are seen to agree well with Taylor's theory, confirming that DDR gives accurate values of interfacial tension for surfactant-free drops. However, the  $c^* = 0.5$  drops all lie above Taylor's theory, implying that the DDR method underestimates the equilibrium interfacial tension. Moreover, the deviation between the dimensionless relaxation times of the  $c^* = 0.5$  drops and Taylor's theory is largest at low  $\lambda^*$  (about 90% at  $\lambda^* = 0.01$ ), and reduces as  $\lambda^*$  increases (about 33% at  $\lambda^* = 3$ ). Thus, from the point of view of applying DDR to measure the interfacial tension of compatibilized drops, Fig. 9 suggests that it

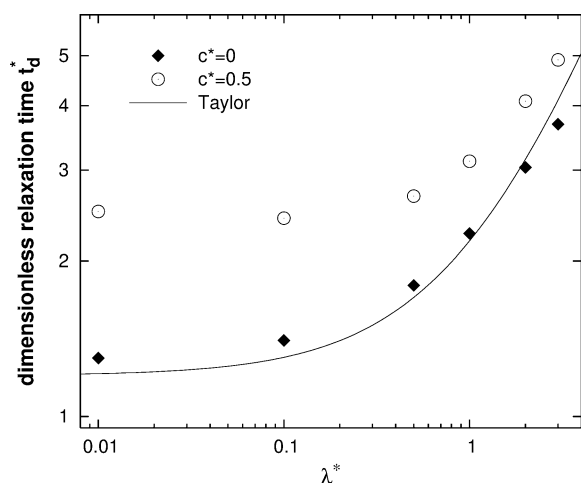


Fig. 9. Dimensionless drop relaxation times  $t_d^*(\lambda^*)$ .

is better to perform measurements on a compatibilized drop with  $\lambda^* > 1$ . This is because the dimensionless relaxation time is closer to that of the surfactant-free drop at high  $\lambda^*$ , and thus the errors due to interfacial tension gradients are reduced.

#### 4. Summary and conclusions

This paper describes simulations of the deformation and retraction of surfactant-laden drops. The deformation history involves a shear strain to deform the drop, followed by retraction under quiescent conditions. An insoluble, nondiffusing surfactant is assumed. The goal of this paper is to assess whether the kinetics of retraction of the drops can yield their equilibrium interfacial tension.

The deformation of the surfactant-laden drop is found to cause gradients in surfactant concentration along its surface. The resulting gradients in interfacial tension affect the retraction behavior significantly.

For large deforming strains, the initial retraction of drops cannot be used to obtain the interfacial tension of drops with surfactant. At high surfactant concentrations, large deviations in the local concentration from the equilibrium value, and corresponding Marangoni stresses, greatly accelerate the initial retraction; thus, an interfacial tension calculated from this retraction using the IFR method is considerably larger than the equilibrium interfacial tension.

For both, small and large deforming strains, the terminal retraction (where the drop may be approximated by a slightly deformed ellipsoid) is affected by the gradients in the surfactant concentration. In particular, at low surfactant concentration two distinct drop relaxation processes are identifiable: a fast shape retraction, and a slow relaxation of interfacial tension gradients. With increasing concentration of surfactant, the slow process becomes faster until it is no longer evident. Analyzing the data in terms of the DDR method, it is found that the ellipsoidal retraction is

considerably slower for surfactant-laden drops. This implies that using DDR underestimates the interfacial tension of surfactant-laden drops. It is shown that the underestimation is most severe at low viscosity ratios.

Finally, it is shown (Appendix B) that the terminal retraction of drops with a linear and a nonlinear constitutive equation can be superposed by expressing the results in terms of the surfactant elasticity. In general, the dynamics of any process involving small deformations of surfactant-laden interfaces, are expected to be independent of the constitutive equation if represented in terms of the surfactant elasticity.

The chief conclusion of this paper is that the dynamics of any process involving large deformation of a surfactant-laden interface are expected to be affected by deviations of the interfacial tension from its equilibrium value. Hence, using the dynamics of such a process to measure the interfacial tension will, in general, yield values that are different from the equilibrium interfacial tension. In particular, the DDR method yields values that are smaller than the equilibrium interfacial tension.

#### Acknowledgments

This work was supported in part by the MRSEC Program of the National Science Foundation under Award DMR-0212302. Additional support was provided by a research Grant (DAAD-19-99-1-0337) from the Army Research Office and from the Industrial Partnership for Research in Interfacial and Materials Engineering (IPRIME: [www.iprime.umn.edu](http://www.iprime.umn.edu)). The authors thank the Supercomputing Institute and the Institute for Mathematics and its Applications (IMA) at the University of Minnesota for computer time. The authors are grateful to Dr. Vittorio Cristini and Dr. John Lowengrub for invaluable discussions.

#### Appendix A. Experimental measurements of interfacial tension

In this section, the experimental details involved in obtaining Fig. 2 are described.

##### A.1. Materials

Some properties of the polymers used for measurement of interfacial tension are given in Table 1. A Haake batch mixer was used to blend 0.2% of the antioxidant Irganox 1010 into the polyethylene before use. Terminal dynamic viscosities (or equivalently, zero shear viscosities) were measured with 25-mm parallel plates in a dynamic stress rheometer (DSR, Rheometric Scientific) at 200 °C. The PS-*b*-PE was synthesized by anionic polymerization followed by catalytic hydrogenation [21], whereas the PS-*b*-PMMA was prepared by atom transfer radical polymerization as described elsewhere [10].

### A.2. Sample preparation and measurements

PS was compression-molded at 200 °C into disks of diameter 31 mm and thickness 1 mm, followed by drying in vacuum at 80 °C. Compression-molding was performed between silicon wafers in order to obtain a smooth and clean surface.

For the PE/PS system, various amounts of PS-*b*-PE (0, 1, 3, and 5 wt%) were mixed at 170 °C with PE in a Minimax Mixer [22] with three steel balls, followed by drawing the melt from the mixer. The resulting fibers of PE with PE-*b*-PS had diameters ranging from 20 to 100 μm. The fibers were placed between two PS disks and then heated in a visualization apparatus to 200 °C for about 1 h. The fibers broke into strings of drops during heating due to capillary instability. For the PMMA/PS system, PMMA spheres of diameter 70–200 μm with PS-*b*-PMMA on the surface were prepared as described elsewhere [10]. These spheres were then embedded between two PS disks by placing them between the disks and heating to 200 °C in the flow visualization apparatus.

PE or PMMA drops embedded in PS disks were then deformed in a parallel plate geometry at a shear rate of  $\sim 1 \text{ s}^{-1}$  using a counterrotating flow visualization apparatus [23]. Shearing was stopped after 4–6 s to prevent breakup of the drop, which occurs beyond a shear strain of about 7. The retraction of the drop back to a spherical shape was recorded using a video camera. For each block copolymer content, drop retraction was measured in at least five independent experiments. Images were digitized by a frame grabber and further analyzed using Scion Image software (Scion Corporation). Analysis consisted of using the edge-detection algorithm in the software, followed by converting the image into a black-and-white image.

### A.3. Analysis of fiber retraction (IFR)

Retraction of the highly elongated drops was analyzed using the procedure suggested by Tjahjadi et al. [20]. Upon cessation of shear, the drop shape was a flat ellipsoid with  $R_1 \gg R_3 > R_2$ . Initial retraction along the vorticity direction caused the drop to become approximately cylindrical with hemispherical end caps with  $R_1 \gg R_3 \approx R_2$ . The time required for the drop to become cylindrical (judged visually) was typically 200–600 s after shearing, depending on the viscosity, drop size, and interfacial tension. This time was denoted time  $t_0$ , and the value of  $R_1$  at this time was taken to be the initial half length of the fiber. The initial radius,  $a(t_0)$ , of the fiber was obtained from Eq. (15), and used to find the initial aspect ratio  $R_1/a(t_0)$ . The initial aspect ratio and  $\lambda^*$  together allow the polynomial coefficients  $k_n$  of Eq. (14) to be determined from Ref. [20]. The dimensionless drop length  $R_1/R_0$  ( $> 1.5$ ) was then plotted vs time  $t$ , and  $\sigma$  in Eq. (14) was chosen to fit the experimental data. Sample fits are shown in Fig. 10a. Note that  $R_1$  is taken to be the longest dimension of the drop when viewed along the gradient di-

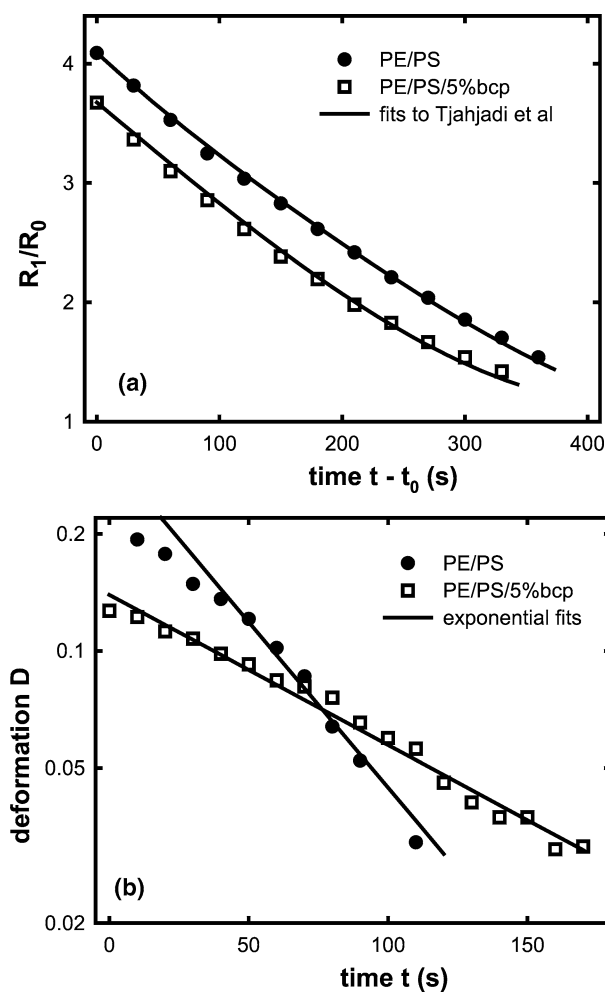


Fig. 10. Experimental determination of interfacial tension by (a) IFR and (b) DDR. Solid lines in (a) and (b) are fits to Eqs. (14) and (17), respectively. Note that (b) has a logarithmic y-axis. The time  $t = 0$  in (b) is arbitrary (see text).

rection whereas in reality, there is some nonzero orientation angle between  $R_1$  and the flow direction. However, due to the small orientation angle and also because  $R_1 \gg$  fiber diameter, this error is small [23].

### A.4. Analysis of drop retraction (DDR)

Interfacial tension was obtained from the terminal stages of retraction using Taylor's small-deformation theory as described by Eqs. (17) and (20). The edge of the drop in the black-and-white picture was fitted to an ellipse using GnuPlot software. It took roughly 400–1000 s after shearing for the drop to become ellipsoidal (judged by quality of fits to the elliptical profile). This time was taken as  $t = 0$  for the DDR method. The drop retraction time  $t_d$  was obtained by fitting Eq. (18) to the exponentially decreasing portion of the deformation vs time data (see Fig. 10b for a typical dataset), and the interfacial tension  $\sigma$  was then obtained from Eq. (20). Due to the small difference between the major and minor axes of the drop, the error caused by the unknown

orientation angle between  $R_1$  and the flow direction represents potentially serious error in this case. Therefore,  $R_1$  was obtained from measurements of  $R_3$  and  $R_0$  by using volume conservation of the drop.

## Appendix B. Linear vs nonlinear surfactants

All the simulations presented in this paper used a nonlinear constitutive equation for surfactant. While the qualitative features of this equation (in particular, “the convex-up” behavior shown in Fig. 4) are expected to be correct on thermodynamic grounds, the equation may not describe the behavior of polymeric surfactants in quantitative detail. It is therefore desirable to represent the data in Figs. 8 and 9 in a form that is independent of constitutive equation, i.e., in this case, independent of  $c^*$ . We propose that the elasticity of the surfactant

$$E^* = - \left( \frac{\Gamma}{\sigma} \frac{\partial \sigma}{\partial \Gamma} \right) \Big|_{\Gamma=\Gamma_e} = - \frac{\partial \log(\sigma)}{\partial \log(\Gamma)} \Big|_{\Gamma=\Gamma_e}, \quad (\text{B.1})$$

is a more appropriate parameter than  $c^*$  to represent the results. This proposition may be tested by comparing the results of the simulations using Eq. (6) with those using an alternative constitutive equation. A linear constitutive equation used previously by numerous other authors (Stone and Leal [24], for example) is

$$\sigma = \sigma_0 - RT\Gamma. \quad (\text{B.2})$$

The parameter  $\beta$  defined by

$$\beta = \frac{RT\Gamma_e}{\sigma_0} \quad (\text{B.3})$$

characterizes the linear surfactant. Using Eq. (B.1) it is easy to show that for a linear surfactant,

$$E^* = \frac{\beta}{1 - \beta}, \quad (\text{B.4})$$

and for the nonlinear surfactant of Eq. (6),

$$E^* = \left( \frac{c^*}{1 - c^*} \right) \frac{E_0^*}{(1 + E_0^* \ln(1 - c^*))}. \quad (\text{B.5})$$

For  $E_0^* = 0.2$ , the values of  $c^* = 0.2, 0.5$ , and  $0.75$  for the nonlinear surfactant give elasticities of  $0.052, 0.23$ , and  $0.83$ , respectively, from Eq. (B.5). These elasticities are matched reasonably well by linear surfactants with  $\beta = 0.05, 0.2$ , and  $0.5$ , respectively. Accordingly, simulations were performed to compare the linear and nonlinear constitutive equations with these parameter values, for drops with  $\lambda^* = 1$ . Fig. 11a compares the deformation parameters for drops with a linear surfactant with  $\beta = 0.2$  ( $E^* = 0.25$ ) and for a nonlinear surfactant with  $E_0^* = 0.2$  and  $c^* = 0.5$  ( $E^* = 0.23$ ). The deformation parameter is virtually identical if the drop is deformed by a strain of 1, whereas there are only minor differences for a deforming strain of 5. Excellent superposition was also obtained for the deformation parameter vs  $t^*$  results upon comparing linear surfactants with  $\beta = 0.05$  and

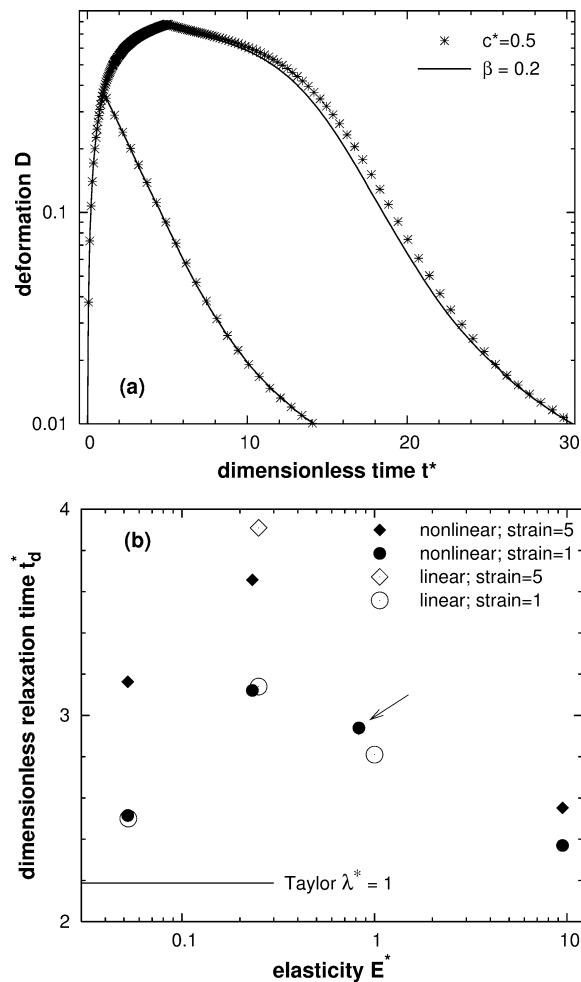


Fig. 11. Retraction of drops with  $\lambda^* = 1$  and linear or nonlinear surfactant constitutive equations. (a) Deformation parameter for drops deformed by a strain of 1 and 5, and (b) dimensionless retraction times; circles and diamonds correspond to strains of 1 and 5 respectively; open and solid symbols correspond to linear and nonlinear constitutive equations, respectively. Solid symbols corresponding to the nonlinear equation are the same points as from Fig. 8a. Also note that a solid diamond and a solid circle coincide at  $E^* = 0.83$  (arrow).

$0.5$  with nonlinear surfactants with  $E_0^* = 0.2$  and  $c^* = 0.2$  and  $0.75$ , respectively (not shown). Fig. 11b shows that the quantity of relevance to the DDR method, the dimensionless drop relaxation time for exponential retraction,  $t_d^*$ , is in excellent agreement for linear and nonlinear surfactants for drops deformed by a strain of 1, and in reasonable agreement for the single case considered at a strain of 5. These results indicate that the elasticity is indeed a suitable parameter to compare results of different constitutive equations.

It must be noted the definition of the elasticity is essentially a local linearization of the relationship between  $\sigma$  and  $\Gamma$ ,

$$\sigma = \sigma_e + \frac{\partial \sigma}{\partial \Gamma} \Big|_{\Gamma=\Gamma_e} (\Gamma - \Gamma_e) = \sigma_e (1 + E^*) - \frac{\sigma_e E^*}{\Gamma_e} \Gamma. \quad (\text{B.6})$$

Thus, the elasticity is a good parameter to compare different constitutive equations only if the concentration of the surfactant on different parts of the drop is sufficiently close to  $\Gamma_e$  so that a linear relationship between  $\sigma$  and  $\Gamma$  is a good approximation. This condition is satisfied for the last stages of drop retraction because regions on the drop surface which had  $\Gamma$  far from the equilibrium concentration initially have had time to approach the equilibrium concentration. The rescaling in terms of elasticity is expected to be unsuccessful when applied to phenomena such as the initial retraction of Fig. 6, or tip streaming [15], in which the local concentration is sufficiently different from  $\Gamma_e$  so that the nonlinear relationship between  $\sigma$  and  $\Gamma$  is evident.

### Appendix C. Nomenclature

$a(t_0)$	Radius of fiber at the start of fiber retraction
$c^*$	Dimensionless equilibrium surface concentration
$k_n$	Polynomial coefficient in the analysis of Tjahjadi et al.
$t$	Time
$t_0$	Time at which fiber retraction starts
$t_d$	Relaxation time of slightly deformed drop
$t_F$	Time for shear flow
$t^*$	Dimensionless time = $\dot{\gamma}t$ during deformation, = $t\sigma_e/(R_0\mu)$ during retraction
$t_d^*$	Dimensionless relaxation time of slightly deformed drop
$t_0^*$	Dimensionless time at which fiber retraction starts
$Ca^*$	Capillary number during shear flow
$D$	Deformation parameter of drop
$E^*$	Elasticity of surfactant
$E_0^*$	Characteristic property of nonlinear surfactant
$\mathbf{n}$	Local outward normal on the surface
$\mathbf{p}_i$	Pressure in fluid $i$ ( $i = d$ or $m$ )
$R_0$	Initial radius of spherical drop
$R_1$	Half of the largest axis of drop
$R_2$	Half of the smallest axis of drop
$R_3$	Half of the axis of drop along the vorticity direction
$\mathbf{T}_i$	Stress tensor in fluid $i$ ( $i = d$ or $m$ )
$\mathbf{u}_i$	Velocity in fluid $i$ ( $i = d$ or $m$ )
$\beta$	Characteristic property of linear surfactant
$\dot{\gamma}$	Shear rate
$\kappa$	Local mean curvature
$\lambda^*$	Ratio of drop viscosity to matrix viscosity
$\mu_m$	Viscosity of matrix
$\mu_d$	Viscosity of drop
$\Gamma$	Interfacial concentration of surfactant
$\Gamma_e$	Interfacial concentration of surfactant on spherical drop at equilibrium
$\Gamma_\infty$	Maximum interfacial concentration of surfactant
$\Gamma^*$	Dimensionless interfacial concentration of surfactant = $\Gamma/\Gamma_e$

$\sigma$	Interfacial tension
$\sigma_e$	Interfacial tension on spherical drop at equilibrium before shearing
$\sigma_0$	Interfacial tension in the absence of surfactant
$\sigma^*$	Dimensionless interfacial tension = $\sigma/\sigma_e$

### References

- [1] P.X. Xing, M. Bousmina, D. Rodrigue, M.R. Kamal, *Macromolecules* 33 (2000) 8020.
- [2] H. Retsos, I. Margiolaki, A. Messaritaki, S.H. Anastasiadis, *Macromolecules* 34 (2001) 5295.
- [3] P.H.M. Elemans, J.M.H. Janssen, H.E.H. Meijer, *J. Rheol.* 34 (1990) 1311.
- [4] J. Kirjava, T. Rundqvist, R. Holstimietinen, M. Heino, T. Vainio, *J. Appl. Polym. Sci.* 55 (1995) 1069.
- [5] D.J. Ihm, J.L. White, *J. Appl. Polym. Sci.* 60 (1996) 1.
- [6] A. Luciani, M.F. Champagne, L.A. Utracki, *J. Polym. Sci. Polym. Phys. Ed.* (1997) 1393.
- [7] K. Okamoto, M. Takahashi, H. Yamane, H. Kashihara, H. Watanabe, T. Masuda, *J. Rheol.* 43 (1999) 951.
- [8] R. Hayashi, M. Takahashi, H. Yamane, H. Jinnai, H. Watanabe, *Polymer* 42 (2001) 757.
- [9] A.S. Almusallam, R.G. Larson, M.J. Solomon, *J. Rheol.* 44 (2000) 1055.
- [10] H.-K. Jeon, C.W. Macosko, *Polymer*, in press.
- [11] S. Velankar, P. Van Puyvelde, J. Mewis, P. Moldenaers, *J. Rheol.* 45 (2001) 1007.
- [12] S. Hansen, G.W.M. Peters, H.E.H. Meijer, *J. Fluid Mech.* 382 (1999) 331.
- [13] Y. Pawar, K. Stebe, *Phys. Fluids* 8 (1996) 1738.
- [14] W.J. Milliken, L.G. Leal, *J. Colloid Interface Sci.* 166 (1994) 275.
- [15] C.D. Eggleton, T.M. Tsai, K.J. Stebe, *Phys. Rev. Lett.* 87 (2001) 48302.
- [16] C.D. Eggleton, Y.P. Pawar, K.J. Stebe, *J. Fluid Mech.* 385 (1999) 79.
- [17] C.W. Macosko, P. Guegan, A.K. Khandpur, A. Nakayama, P. Marechal, T. Inoue, *Macromolecules* 29 (1996) 5590.
- [18] H. Zhou, V. Cristini, C.W. Macosko, J. Lowengrub, submitted for publication.
- [19] V. Cristini, J. Blawdziewicz, M. Loewenberg, *Phys. Fluids* 10 (1998) 1781.
- [20] M. Tjahjadi, H.A. Stone, J.M. Ottino, *J. Fluid Mech.* 243 (1992) 297.
- [21] F.S. Bates, J.H. Rosedale, H.E. Bair, T.P. Russell, *Macromolecules* 22 (1989) 2557.
- [22] M. Maric, C.W. Macosko, *Polym. Eng. Sci.* 41 (2001) 118.
- [23] L. Levitt, C.W. Macosko, S.D. Pearson, *Polym. Eng. Sci.* 36 (1996) 1647.
- [24] H.A. Stone, L.G. Leal, *J. Fluid Mech.* 220 (1990) 161.
- [25] H. Gramespacher, J. Meissner, *J. Rheol.* 36 (1992) 1127.
- [26] P.C. Ellingson, D.A. Strand, A. Cohen, R.L. Sammler, C.J. Carriere, *Macromolecules* 27 (1994) 1643.
- [27] K. Okamoto, M. Takahashi, H. Yamane, H. Watashiba, Y. Tsukahara, T. Masuda, *Nihon Reoroji Gakkaiishi* 27 (1999) 109.
- [28] Y.T. Hu, A. Lips, *Phys. Rev. Lett.* 91 (2003) 044501.
- [29] V. Cristini, J. Blawdziewicz, M. Loewenberg, *J. Comp. Phys.* 168 (2001) 445.
- [30] V. Cristini, R.W. Hooper, C.W. Macosko, M. Simeone, S. Guido, *Ind. Eng. Chem. Res.* 41 (2002) 6305.